Publ. Astron. Soc. Japan 39, 559–571 (1987)

A Magnetodynamical Model for the Galactic Center Lobes

Kazunari SHIBATA

Department of Earth Sciences, Aichi University of Education, Kariya, Aichi 448

and

Yutaka UCHIDA*

Tokyo Astronomical Observatory, University of Tokyo, Mitaka, Tokyo 181

(Received 1986 July 16; accepted 1987 February 16)

Abstract

We present an MHD model for the galactic center lobes (GCL) by using an axisymmetric 2.5-dimensional MHD simulation. According to our model, GCL is a low-energy jet emanating from the H II gas disk extending beyond $r\sim 100$ pc from the galactic center. The model is based on the "sweeping-magnetic-twist" mechanism developed by the authors for the production of cosmic jets, where the gas in the surface layer of the contracting disk is lifted up by the $\boldsymbol{J}\times\boldsymbol{B}$ force in the relaxing magnetic twist, which is generated by the interaction of the rotation of the contracting disk with the poloidal magnetic field. We incorporate the realistic gravitational potential suitable for the galactic center region, in which the rotational velocities are approximately constant for $r=20$–100 pc. The difference between the models with this realistic potential and those with the potential due to a point mass is examined in detail. On the basis of the numerical results, we present a scenario for the formation of the GCL.

Key words: Astrophysical jets; Galactic center; Twisted magnetic fields.

1. Introduction

Sofue and Handa (1984) found a prominent lobe with a size of about 100 pc above the center of our Galaxy in the radio continuum survey at 10 GHz performed at Nobeyama. This galactic center lobe, which is hereafter referred to as the GCL, has an appearance of a pair of ox-horns in projection, or a hollow cylindrical shell structure in three dimensions, and seems to emanate from the galactic center H II gas disk (Mezger and Pauls 1979; Liszt and Burton 1979). Sofue (1984, 1985) suggested that the GCL may be a low-energy prototype of radio jets observed in the active galaxies and quasars (e.g. Begelman et al. 1984; Bridle and Perley 1984), and constructed a model in which the GCL is regarded as the shock front originating

* Present address: Department of Astronomy, Faculty of Science, University of Tokyo, Bunkyo-ku, Tokyo 113.

from the explosion at the galactic nucleus. On the other hand, it is well known that there is a peculiar structure called "radio arc" which seems to be connected to the galactic nucleus Sgr A. The arc has an apparent size of about 50 pc, and its vertical branch is located just along the extension of the eastern ridge of the GCL. The oblique branch of the arc connects the vertical branch to Sgr A. According to a recent VLA observation with a high spatial resolution (Yusef-Zadeh et al. 1984; Morris and Yusef-Zadeh 1985), this arc shows a significant filamentary structure suggesting some effects of a magnetic field. Indeed, more recent observations of radio polarization (Inoue et al. 1984; Tsuboi et al. 1985, 1986; Seiradakis et al. 1985) have confirmed the presence of a strong magnetic field parallel to the vertical branch of the arc. The polarization observations revealed that the directions of the magnetic vectors corrected for the Faraday rotation lie just along the eastern ridge of the GCL, and the line-of-sight component of the magnetic field along the eastern ridge of the GCL (passing through the vertical branch of the arc) changes sign across the galactic plane (Inoue et al. 1984; Tsuboi et al. 1985).

As for the western ridge of the GCL, there is no strong Faraday rotation measure (M. Inoue 1985, private communication), although the filamentary structure is also found at Sgr C at the foot of the western ridge of the GCL (Listz 1985).

These observations strongly suggest that the GCL may be a manifestation of the activity related to the strong magnetic field in the galactic center region. Hence, Uchida et al. (1985) proposed an MHD model for the GCL, in which the gas in the GCL is lifted up from the H II gas disk by the $\boldsymbol{J}\times\boldsymbol{B}$ force in the relaxing magnetic twists, which are generated by the interaction of the rotating H II gas disk in contraction with the poloidal magnetic field lines. This model is based on the MHD model for the astrophysical jets developed by the present authors, named the "sweeping-magnetic-twist" mechanism (Uchida and Shibata 1985a, b, c, 1986; Shibata and Uchida 1985, 1986a, b). This model agrees well with various observational facts about the GCL, such as the morphology of the GCL [the cylindrical shell structure found by Sofue and Handa (1984)], and the polarization features found by Inoue et al. (1984) and Tsuboi et al. (1985) described above. For example, the opposite sign of the line-of-sight component of the magnetic field above and below the galactic plane is naturally explained as the helically twisted magnetic field lines which are pulled by the rotation of the gas disk in the direction of the galactic rotation (Uchida et al. 1985).

In Uchida et al. (1985), the gravitational potential in the galactic center region is assumed for simplicity to be the one produced by a point mass. Such a potential due to a point-mass is hereafter called the Kepler potential. The observation of the rotational velocity in the galactic center region, however, shows that the rotational velocity is approximately constant between the radial distances of 50 pc and of 200 pc from the galactic nucleus (Sgr A) (e.g. Oort 1977). If this rotational velocity is the result of the balance between the centrifugal and the gravitational forces, the gravitational potential in the galactic center region is not the Kepler one. In the present paper, we extend the scheme proposed by Uchida et al. (1985) to the case with a more realistic gravitational potential suitable for the galactic center region and see what kind of modifications follow from this.

Section 2 describes the fundamental assumptions, basic equations, and numerical methods. The results are given in section 3 and a scenario on the formation of the GCL and the related problems are discussed in section 4.

2. Assumptions, Basic Equations, and Numerical Methods

The situations considered in the MHD model of Uchida et al. (1985) are as follows [see also Uchida and Shibata (1985a, b, c) and Shibata and Uchida (1986a, b)]. Initially, we consider a dense, warm isothermal gas disk (H II gas disk) with a uniform magnetic field penetrating the disk vertically, i.e., parallel to the rotation axis of the disk. A hydrostatic isothermal halo is assumed outside the disk. Then, let the disk rotate with a sub-Keplerian rotational velocity. The disk pulls the magnetic field lines toward the center as well as in the φ direction, generating the magnetic twists. As the disk contracts, the magnetic field is tightly twisted. When the magnetic twist becomes sufficiently large, the gas in the surface layers of the disk starts to be accelerated upward above the disk and downward below the disk, producing supersonic jets (GCL). The resulting jets have a hollow cylindrical shell structure spinning around the axis of rotation.

Here in this paper, we consider the same situation as the above and adopt various possible forms for the gravitational potential. In order to model these situations numerically, we assume (1) 2.5-dimensional axisymmetry around the rotation axis of the disk, where 2.5-dimensional means $\partial/\partial\varphi=0$ in the cylindrical coordinates but v_φ and B_φ are not zero, (2) ideal MHD (adiabatic, infinite electrical conductivity), and (3) that the self-gravity of the disk is neglected. The basic equations are as follows:

$$\frac{\partial\rho}{\partial t}+\nabla\cdot(\rho\boldsymbol{V})=0\,, \tag{1}$$

$$\rho\frac{d\boldsymbol{V}}{dt}+\nabla p-\frac{1}{4\pi}(\nabla\times\boldsymbol{B})\times\boldsymbol{B}-\rho\boldsymbol{g}=0\,, \tag{2}$$

$$\frac{\partial\boldsymbol{B}}{\partial t}-\nabla\times(\boldsymbol{V}\times\boldsymbol{B})=0\,, \tag{3}$$

$$\frac{d}{dt}(p\rho^{-\gamma})=0\,, \tag{4}$$

where

$$\frac{d}{dt}\equiv\frac{\partial}{\partial t}+\boldsymbol{V}\cdot\nabla$$

and $\boldsymbol{g}=-\text{grad}\,\psi$ is the gravitational acceleration vector due to the potential ψ, which is described later in this section, and γ is the ratio of specific heats.

The initial conditions are the same as those in the previous model described above. For practical reasons in the calculations, we set an inner spherical boundary at $(r^2+z^2)^{1/2}=r_\mathrm{b}=0.3\times r_\mathrm{d}$ surrounding the origin, where r_d is the inner radius of the initial

disk. The boundary conditions on this inner boundary and on the top and side surfaces of the cylindrical region are all assumed to be the free boundary conditions. The basic equations are made dimensionless and as a result we have the following dimensionless parameters:

$$R_1=(V_s/V_p)^2 , \tag{5}$$

$$R_2=(V_A/V_p)^2 , \tag{6}$$

$$R_3=(V_{\varphi 0}/V_p)^2 , \tag{7}$$

$$R_4=T_{halo}/T_{disk} , \tag{8}$$

where V_s, V_A, and $V_{\varphi 0}$ are respectively the sound, Alfvén, and rotational velocities at $r=r_d$ in the initial disk, and V_p is the rotational velocity satisfying the balance between the centrifugal and gravitational forces at $r=r_d$ in the model potential, T_{halo} and T_{disk} are the initial temperatures of the halo and the disk, respectively. [If the potential is the one produced by a point mass, V_p becomes the Kepler velocity as in the previous papers (e.g., Shibata and Uchida 1986a, b)]. The length, the velocity, and the time are normalized by r_d, V_p, and r_d/V_p. Other normalization factors such as ρ_d (density), T_d (temperature), and B_0 (magnetic field strength) are all those at $r=r_d$ on the equatorial plane of the initial disk. We adopt the normalization factors for these quantities, (r_d, ρ_d, T_d, V_p, B_0) suitable for the GCL as (100 pc, 10^{-23} g cm^{-3}, 5000 K, 200 km s^{-1}, 2×10^{-5} G). Then, the dimensionless parameters become (R_1, R_2, R_4)= (1.8×10^{-3}, 4.3×10^{-3}, 400), if T_{halo} is assumed to be 2×10^6 K. We assume that R_3 is smaller than unity (sub-Keplerian rotation for the initial disk), but the exact value

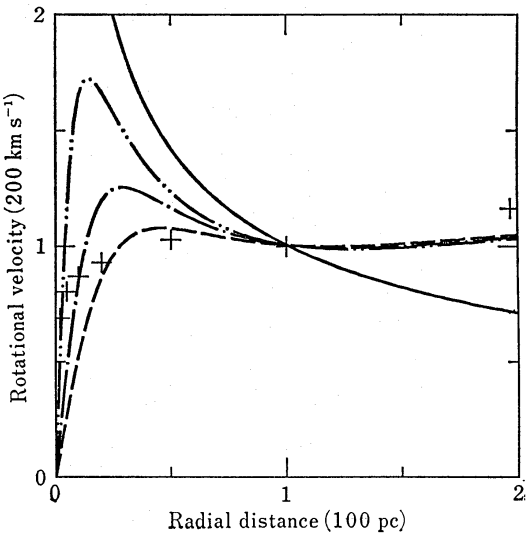

Fig. 1. The rotation curves for modified Plummer's (1915) potential ($b_1=0.3$: dashed curve; 0.2: dash-dotted curve; and 0.1: dash-double dotted curve). The curve for the Kepler potential (KP) is also shown by the solid curve. The crosses denote the observed distribution of rotational velocities (Oort 1977). The case of $b_1=0.3$ in modified Plummer's (1915) potential is called in the text the flat rotation potential (FRP). The units of the velocity and the length are V_p (=200 km s^{-1}) and r_d (=100 pc), respectively.

of R_3 is taken to be a free parameter. The numerical values quoted in later sections are all dimensionless ones defined in this section unless otherwise noted.

As the gravitational potential suitable for the galactic center region, we assume a linear combination of Plummer's (1915) potentials given by

$$\phi=c_2[c_1/(R^2+\tilde{b}_1^2)^{1/2}+(1-c_1)/(R^2+\tilde{b}_2^2)^{1/2}]\,, \tag{9}$$

where $R=(r^2+z^2)^{1/2}$ is the distance from the galactic nucleus (Sgr A), and c_1, c_2, $\tilde{b}_1$, and $\tilde{b}_2$ are free parameters, which are determined by the condition that the distribution of the rotational velocity approximates the observed one in the galactic center region, when the rotation satisfies the balance between the centrifugal and gravitational forces in this potential. According to Oort (1977), the rotational velocity of the gas disk around $r=50$–200 pc in the galactic center region is approximately constant $\sim 200\ \mathrm{km\ s^{-1}}$. Assuming that $c_1=0.75$ and $b_2=\tilde{b}_2/r_\mathrm{d}=3.0$, we seek $b_1=\tilde{b}_1/r_\mathrm{d}$ which best approximates the observed flat profile of the rotational velocity. Note that c_2 is determined by the condition that $V_\mathrm{p}=200$ km at $r=r_\mathrm{d}=100$ pc. Figure 1 shows the distributions of the rotational velocity for both observations (crosses) and models (others). The case in the Kepler potential is also shown in this figure by solid curves. Model curves for three cases are shown: $b_1=0.1$, 0.2, and 0.3. It is found from this figure that the case $b_1=0.3$ best agrees with the observed curve. Thus, in later sections we mainly study the case $b_1=0.3$ for the model of the GCL.

3. Numerical Results

3.1. *Characteristic Properties of the Model in the Case of the Gravitational Potential Producing a Flat Rotation Curve*

We now show the results in the case of the gravitational potential shown in figure 1 suitable for the galactic center (the potential with $b_1=0.3$). We show in figures 2a through 2e the time development of ρ, the density, $\boldsymbol{V}_{/\!/}=(V_r, V_z)$, the poloidal velocity vector, $\boldsymbol{B}_{/\!/}=(B_r, B_z)$, the poloidal field lines, V_φ, the azimuthal velocity, and B_φ, the azimuthal component of the magnetic field, for the case of $(R_1, R_2, R_3, R_4)=(1.8\times 10^{-3}, 4.3\times 10^{-3}, 0.49, 400)$ (see section 2).

As seen in figure 2, the disk contracts toward the center and rotates around the axis of rotation as well, and pulls the field lines in both these directions. The magnetic field is helically twisted by the rotation of the disk. When the generated magnetic twist relaxes along the poloidal field lines, the gas in the surface layers of the disk is lifted up by the $\boldsymbol{J}\times\boldsymbol{B}$ force. The gas ejected from the disk has a hollow cylindrical shell structure. These dynamical processes are essentially the same as those in the case of the Kepler potential presented in the previous papers (e.g., Uchida et al. 1985).

In order to compare the above result with the case of the Kepler potential in more detail, we show in figure 3 the latter case where all the parameters are set equal to those in the former case except for the potential form. Hereafter, we use the abbreviations for the case of the "flat rotation potential" as FRP and for the case of the Kepler potential as KP. By carefully comparing figure 2 with figure 3, we find the following points:

(1) The velocity of the ejected mass (jet) is larger in the KP case than that in

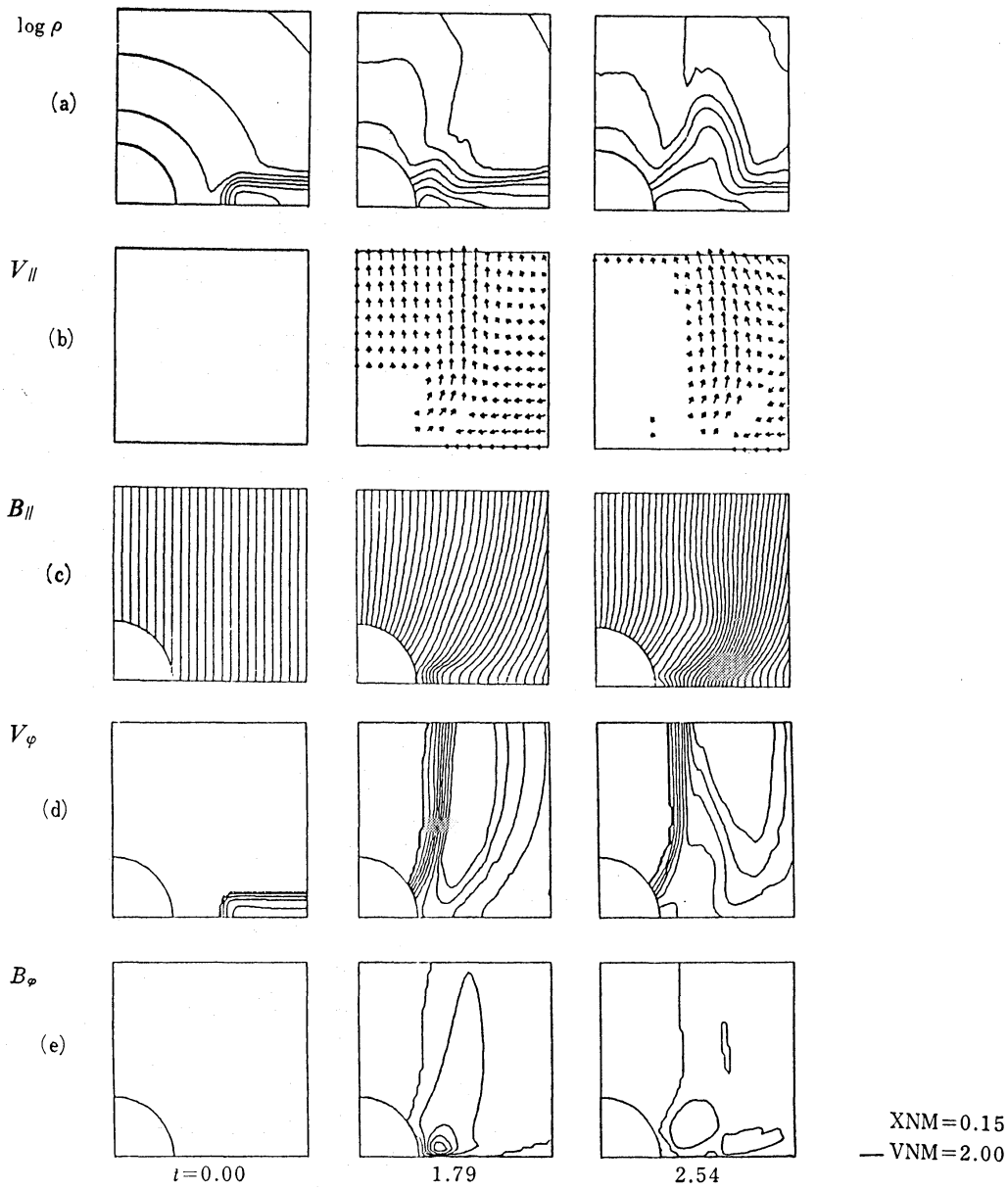

Fig. 2. Time variations of (a) $\log\rho$ (density), (b) $V_{//}=(V_r, V_z)$ (poloidal velocity vector), (c) $B_{//}=(B_r, B_z)$ (poloidal magnetic field lines), (d) V_φ (azimuthal velocity), and (e) B_φ (azimuthal component of the magnetic field) in the case of the flat rotation potential (FRP) with $(R_1, R_2, R_3, R_4; b_1)=(1.8\times10^{-3}, 4.3\times10^{-3}, 0.49, 400; 0.3)$. The scale of the velocity vector is shown by the short line on the right-hand margin of the figure of $t=2.54$ in units of $0.85V_p$ $(=170\ \mathrm{km\ s^{-1}})$; VNM=2.0 indicates that the arrow with the length of this line has the velocity of $2.0\times0.85\ V_p$ $(=340\ \mathrm{km\ s^{-1}})$. Similarly, the scale of the length is also shown by this short line in units of r_d. The whole size of the region illustrated in these figures is $(r_{max}\times z_{max})=(1.3\times1.3)$. The contour-level step width is 0.5 for (a) in the logarithmic scale, 0.2 for (d) in units of $0.85\ V_p$, 1.0 for (e) in units of $B_z\,(t=0)$, The numbers below each frame represent the time in units of the free fall time $(=r_d/V_p=5\times10^5\ \mathrm{yr})$.

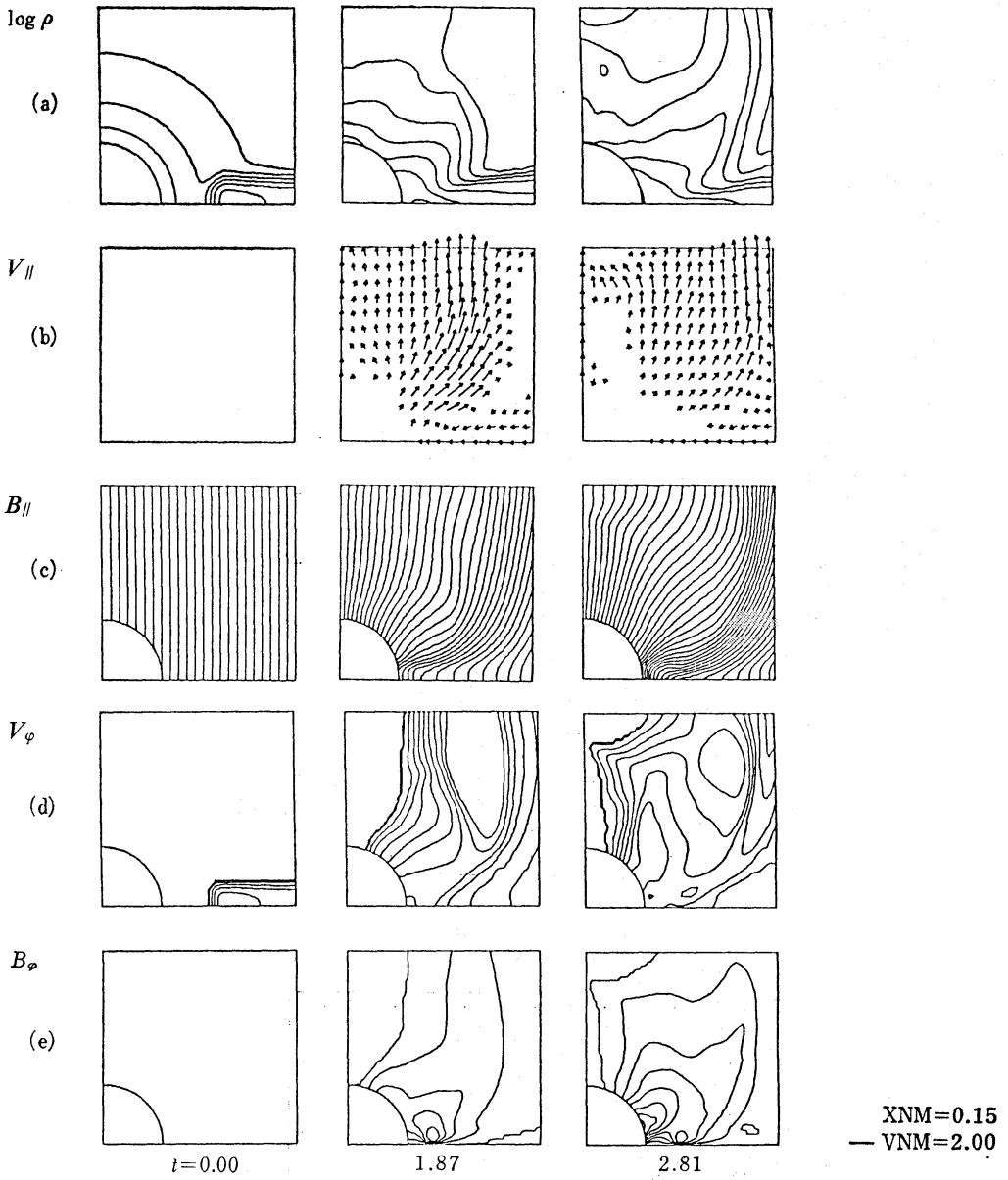

Fig. 3. Time variations of (a) $\log\rho$ (density), (b) $V_{//}=(V_r, V_z)$ (poloidal velocity vector), (c) $B_{//}=(B_r, B_z)$ (poloidal magnetic field lines), (d) V_φ (azimuthal velocity), and (e) B_φ (azimuthal component of the magnetic field) in the case of the Kepler potential (KP) with $(R_1, R_2, R_3, R_4)=(1.8\times10^{-3}, 4.3\times10^{-3}, 0.49, 400)$. Other remarks are the same as in figure 2.

the FRP case by about a factor 2–3.

(2) The contraction of the disk is strongly decelerated or stopped in FRP, while the disk continues to contract in KP.

(3) The maximum value of the azimuthal component of the magnetic field is larger in KP than that in FRP by a factor larger than 2. In fact, B_φ has almost vanished at $t=2.54$ of figure 2f, while it keeps a large value at all times in KP (figure 3f).

The physical reason for (1) is the following. The gravitational energy released in the contraction of the disk is smaller in FRP than in KP due to the softness of the

potential around the center. This leads to the smaller velocity of the jet in FRP, since the kinetic energy of the jet comes from the gravitational energy released in the contraction of the disk in our jet model.

Next, we consider the reason for (2), i.e., why the contraction of the disk is strongly decelerated or stopped. In order to see the mechanism for this, we show in figure 4 the distribution of the rotational velocity along r on the equatorial plane for both KP and FRP. Figure 4a corresponds to FRP and 4b to KP. The solid curves denote $V_p(r)$'s, the rotational velocities that exactly satisfy the centrifugo-gravitational equilibrium, and the other curves are the numerical results at different times. We see that the rotational velocties in the numerical results at $t=2.54$ are approximately equal to

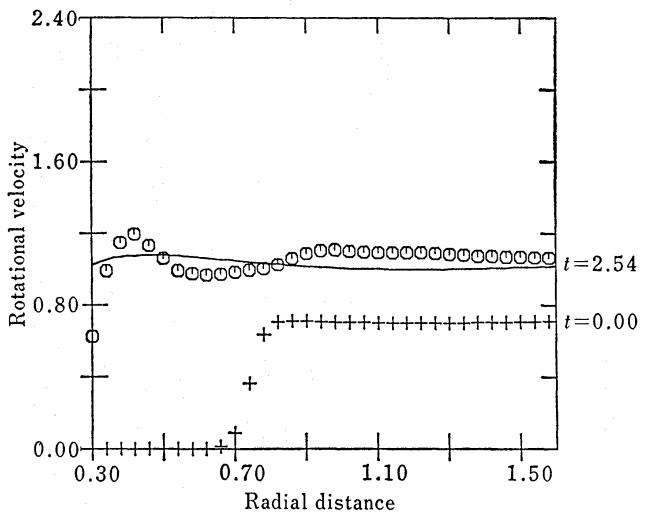

(a)

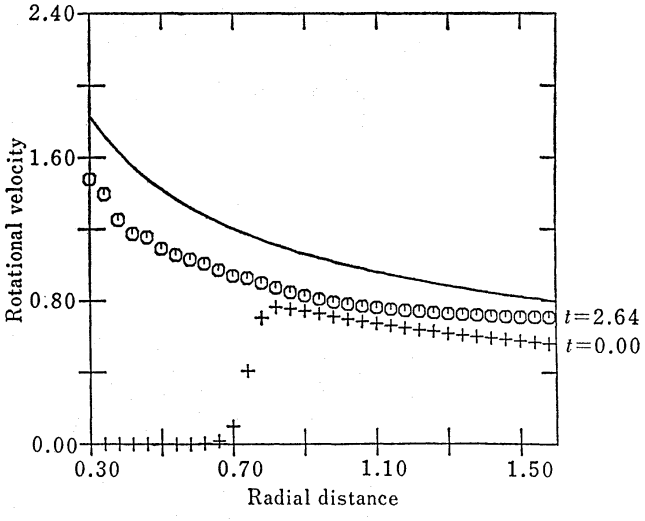

(b)

Fig. 4. The distributions in r of the rotational velocities of the gas in the disk at $z=0$ (the equatorial plane). (a) FRP case ($t=0.0$: crosses; $t=2.54$: circles) corresponding to figure 2 and (b) KP case ($t=0.0$: crosses; $t=2.64$: circles) corresponding to figure 3. The solid curves for both (a) and (b) represent the rotational velocities in the centrifugo-gravitational equilibrium.

the equilibrium values (solid curve) in FRP. This is the reason why the disk is decelerated or stopped after the initial contraction. On the other hand, the rotational velocity always stays below the equilibrium value in KP. Thus, the disk can continue to contract toward the center in KP. This is because the specific angular momentum of the disk gas is carried away by the magnetic effect during the contraction (magnetic braking), while without it the actual rotation increases over the centrifugal equilibrium curve and the contraction is stopped. The angular momentum loss by magnetic braking allows the disk to continue the contraction in KP. What we must emphasize is that in FRP the angular momentum extraction from the disk through the magnetic field with moderate strength is not sufficient to make the disk contract indefinitely. Contraction cannot continue in FRP, because the rotational velocity overshoots the equilibrium value even with magnetic braking, since the equilibrium velocity curve in FRP is flat and low. Figure 4a shows another interesting fact in relation to the angular momentum problem; the dip in the rotation curve in the FRP case, where V_φ's are systematically smaller than the equilibrium values, is located just in the region at the foot of the jet. That is, the angular momentum loss due to the magnetic torque is enhanced by the production of the jet as noted in Shibata and Uchida (1986b).

Third, we consider the reason for (3): the azimuthal component of the magnetic field is smaller in FRP than in KP. This is simply the manifestation of the difference in the rotational velocity of the disk gas, i.e., in the inner region ($r<1.0$) the rotational velocity in equilibrium is smaller in FRP than in KP. Thus, the twisting of the magnetic field is weaker in FRP than in KP.

The results (1) and (2) in this section suggest further that the structure like the GCL can be a transient one for FRP, intermittently ejected and then falling back on the disk, while a new one is being produced when new gas is supplied to the disk from larger r by losing angular momentum (see section 4).

3.2. Parameter Dependence on the Solution

We have calculated several cases by changing the free parameter $R_3[=(V_{\varphi 0}/V_p)^2]$. Note that the parameter R_3 indicates the degree of the sub-Keplerian rotational velocity in the initial state. In this subsection, we summarize the results briefly.

We show in figure 5 four cases with different R_3's: $R_3=0.25$, 0.49, 0.64, and 0.81. Other parameters are fixed: $(R_1, R_2, R_4; b_1)=(1.8\times10^{-3}, 4.3\times10^{-3}, 400; 0.3)$. We can see that the velocity of the jet significantly increases with decreasing R_3. When $R_3=0.81$, there is no prominent mass ejection as seen in the velocity field of figure 5. The result in the case with $R_3=0.25$ shows the production of a prominent jet similar to that shown in figure 3 (the case of KP but with $R_3=0.49$). Thus, we can conclude that even in FRP we have results similar to those in KP by decreasing the value of parameter R_3.

4. Discussion

We have shown in previous sections that the velocity of the jet produced by the sweeping-magnetic-twist mechanism (Uchida and Shibata 1985a, b; Shibata and

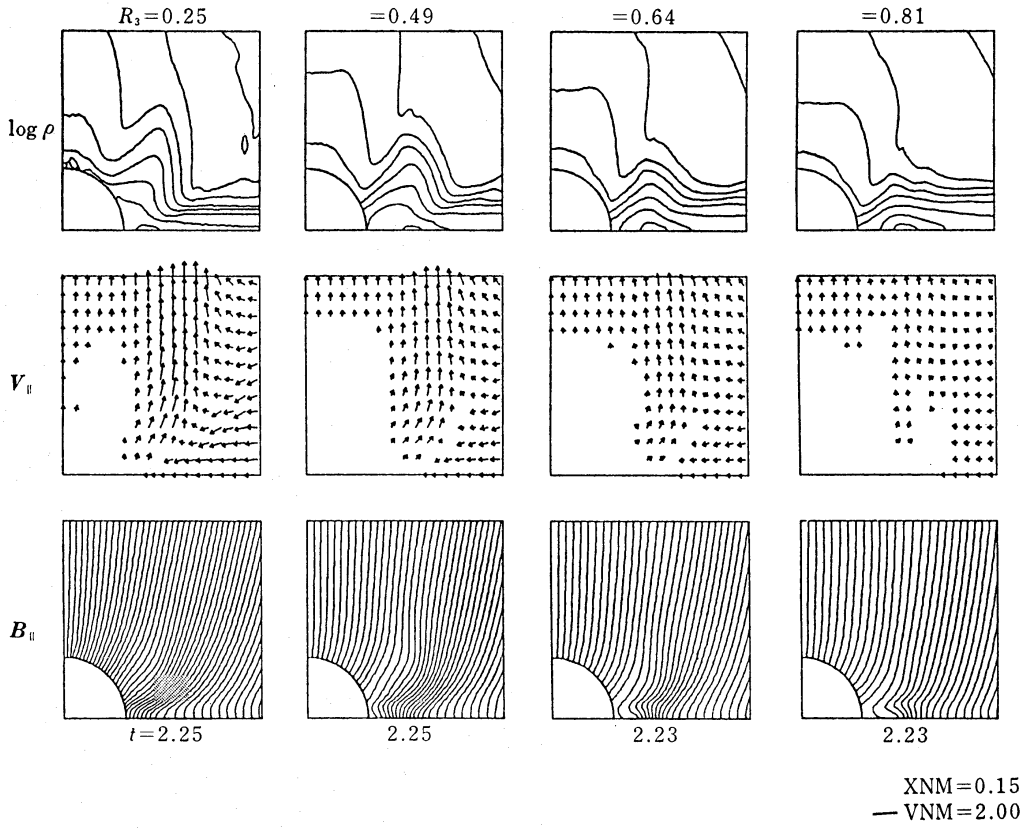

Fig. 5. Parameter dependence of the numerical results upon the parameter $R_3=(V_{\varphi 0}/V_p)^2$. These figures show the distributions of log ρ, $V_{//}$, and $B_{//}$ at the time when the jets are developed (t=2.23–2.25). The other parameters are fixed to be $(R_1, R_2, R_4; b_1)=(1.8\times10^{-3}, 4.3\times10^{-3}, 400; 0.3)$. Other remarks are the same as in figure 2.

Uchida 1985, 1986a, b) is smaller for the flat-rotation-potential (FRP) case than the case with a Kepler potential (KP). There is no prominent jet when the initial rotational velocity of the disk is close to the one in the centrifugo-gravitational equilibrium. In order to produce a prominent jet in FRP suitable for the galactic center, the initial rotational velocity should be smaller than that in the centrifugo-gravitational equilibrium: $R_3=(V_{\varphi 0}/V_p)^2<0.5$. If this initial condition for the disk is satisfied, a hollow cylindrical jet similar to the GCL is produced as a result of the interaction between the poloidal magnetic field and the contraction of the rotating disk through the sweeping-magnetic-twist mechanism proposed by the authors.

Considering these, we present the following scenario for the formation of the GCL. The H II gas disk rotating at $r\sim$a few hundred parsecs first starts falling towards the center by losing a large amount of its angular momentum by some mechanism, e.g., the gravitational torque exerted in passing through a barred potential (Sørenson et al. 1976) or a triaxial potential (Habe and Ikeuchi 1985) in the region surrounding the galactic nucleus. As a result, the rotation of the disk diminishes to smaller values so that $R_3=(V_{\varphi 0}/V_p)^2<0.5$ when it reaches $r\sim100$ pc. As the disk falls towards a smaller radius, the magnetic field lines are tightly twisted by the rotation of the infalling disk. Then, the gas in the surface layers of this H II gas disk is

lifted up by the $\boldsymbol{J}\times\boldsymbol{B}$ force to produce a hollow cylindrical jet (GCL) when the magnetic twist relaxes along the poloidal field. The initial velocity of gas in the GCL is of the order of 100 km s^{-1}. Since the gravitational potential is nearly spherically symmetric or axially symmetric at $r=10$–100 pc in the galactic center, the amount of angular momentum lost from that part of the disk is not large. (The rate of the angular momentum loss through the magnetic torque is small.) Thus the disk ceases to fall at $r=10$–50 pc. This state may be what we see. The time scale for this process is a dynamical one, $\sim 10^6$ yr. Similar radio lobes found in other spiral galaxies (e.g., Duric et al. 1983; Hummel et al. 1983) may also be explained by the sweeping-magnetic-twist mechanism, although the time scales and the sizes may be different from that of the GCL due to different physical conditions.

Finally, we comment on several points obtained from the detailed observations of the GCL. First, the structure of the GCL is highly asymmetric with respect to both the equatorial plane and the axis of galactic rotation. Both asymmetries are not necessarily inconsistent with our model, because the essence of our model is based on the interaction of the magnetic field with the contraction of the H II gas disk, and the axisymmetry is assumed for the convenience of the treatment. In particular, the distance between the nucleus (Sgr A) and the two (west and east) ridges of the GCL is considerably different. This asymmetry is difficult to explain by the models based on a single and simultaneous activity such as an explosion occurred at Sgr A (e.g., Sofue 1984). On the other hand, the energy in our model jet comes from the release of the potential energy of the disk situated at around $r=10$–100 pc; i.e., our model is based on a large-scale gravitational potential which may be asymmetric with respect to Sgr A, because the potential around $r=10$–100 pc is produced by the stellar mass and not affected much by the mass located at the galactic center. (The total stellar mass included in the region is estimated to be 10^8–$10^9 M_\odot$, while the mass at the center is considered to be about $10^6 M_\odot$.)

The second problem is the origin of the enigmatic structures and activities related to the radio arc (Yusef-Zadeh et al. 1984; Inoue et al. 1984; Tsuboi et al. 1985, 1986; Morris and Yusef-Zadeh 1985; Seiradakis et al. 1985; Yusef-Zadeh et al. 1986b). From the observations that there is no strong polarization in the western ridge of the GCL, Tsuboi et al. (1986) suggested that the western and eastern ridges are physically independent phenomena, because in the eastern ridge strong nonthermal emissions and polarizations are found (Tsuboi et al. 1985, 1986; Seiradakis et al. 1985; Yusef-Zadeh et al. 1986b). As evidence supporting their argument, they further referred to the infrared observations (Gautier et al. 1984; Little and Price 1985) that show a lobe structure just on the western ridge of the GCL. However, we consider that the nonthermal emission at the eastern ridge is a secondary phenomenon and the difference between the eastern and western ridges may not be essential for the origin of the GCL, since the infrared lobe on the western ridge of the GCL is explained as a low-energy jet driven by the $\boldsymbol{J}\times\boldsymbol{B}$ force in our model. The basic structure of the GCL may be produced by the sweeping-magnetic-twist mechanism, and the nonthermal electrons are injected from Sgr A to the radio arc, and provide the part of the eastern ridge of the GCL with high-energy electrons which give rise to the polarized nonthermal emission. In fact, the radio arc seems to be physically connected to Sgr A

with some filamentary bridges, which possibly delineate magnetic field lines (Yusef-Zadeh et al. 1984). In this connection, Sofue and Fujimoto (1987) suggest that Sgr A has jets precessing around (e.g., Fukui et al. 1977; Yusef-Zadeh et al. 1986a; Sofue et al. 1986) and one of them interacts with the poloidal magnetic field of the GCL to produce energetic electrons which light up the structures of the radio arc. We also consider that a part of the GCL is illuminated by the nonthermal electrons provided from Sgr A through the radio arc, or by the magnetic reconnection in the radio arc itself.

The authors acknowledge the valuable discussions with Drs. Y. Sofue, S. Ikeuchi, F. Takahara, M. Fujimoto, Y. Fukui, M. Inoue, T. Handa, M. Tsuboi, and M. Umemura. Computations were performed on FACOM M380R at the Tokyo Astronomical Observatory, on FACOM M380R at the Nobeyama Radio Observatory, and on FACOM M200 and VP100 at the Institute of Plasma Physics, Nagoya University. This work was supported in part by the Scientific Research Fund of the Ministry of Education, Science, and Culture (60740130 and 61740139).

References

Begelman, M. C., Blandford, R. D., and Rees, M. J. 1984, *Rev. Mod. Phys.*, **56**, 255.
Bridle, A. H., and Perley, R. A. 1984, *Ann. Rev. Astron. Astrophys.*, **22**, 319.
Duric, N., Seaquist, E. R., Crane, P. C., Bignell, R. C., and Davis, L. E. 1983, *Astrophys. J. Letters*, **273**, L11.
Fujimoto, M. and Sofue, Y. 1986, **11**, 000.
Fukui, Y., Iguchi, T., Kaifu, N., Chikada, Y., Morimoto, M., Nagane, K., Miyazawa, K., and Miyaji, T. 1977, *Publ. Astron. Soc. Japan*, **29**, 643.
Gautier, T. N., Hauser, M. G., Beichman, C. A., Low, F. J., Neugebauer, G., Rowan-Robinson, M., Aumann, H. H., Boggess, N., Emerson, J. P., Harris, S., Houck, J. R., Jennings, R. E., and Marsden, P. L. 1984, *Astrophys. J. Letters*, **278**, L57.
Habe, A., and Ikeuchi, S. 1985, *Astrophys. J.*, **289**, 540.
Hummel, E., van Gorkom, J. H., and Kotanyi, C. G. 1983, *Astrophys. J. Letters*, **267**, L5.
Inoue, M., Takahashi, T., Tabara, H., Kato, T., and Tsuboi, M. 1984, *Publ. Astron. Soc. Japan*, **36**, 633.
Liszt, H. S. 1985, *Astrophys. J. Letters*, **293**, L65.
Liszt, H. S., and Burton, W. B. 1979, in *The Large Scale Characteristics of Galaxy, IAU Symp. No. 84*, ed. W. B. Burton (Reidel, Dordrecht), p. 343.
Little, S. J., and Price, S. D. 1985, *Astron. J.*, **90**, 1812.
Mezger, P. G., and Pauls, T. 1979, in *The Large Scale Characteristics of Galaxy, IAU Symp. No. 84*, ed. W. B. Burton (Reidel, Dordrecht), p. 357.
Morris, M., and Yusef-Zadeh, F. 1985, *Astron. J.*, **90**, 2511.
Oort, J. H. 1977, *Ann. Rev. Astron. Astrophys.*, **15**, 295.
Plummer, H. C. 1915, *Montly Notices Roy. Astron. Soc.*, **76**, 107.
Seiradakis, J. H., Lasenby, A. N., Yusef-Zadeh, F., Wielebinsky, R., and Klein, U. 1985, *Nature*, **317**, 697.
Shibata, K., and Uchida, Y. 1985, *Publ. Astron. Soc. Japan*, **37**, 31.
Shibata, K., and Uchida, Y. 1986a, *Astrophys. Space Sci.*, **118**, 443.
Shibata, K., and Uchida, Y. 1986b, *Publ. Astron. Soc. Japan*, **38**, 631.
Sofue, Y. 1984, *Publ. Astron. Soc. Japan*, **36**, 539.
Sofue, Y. 1985, *Publ. Astron. Soc. Japan*, **37**, 697.
Sofue, Y., and Fujimoto, M. 1987, *Astrophys. J. Letters*, **319**, L73.

Sofue, Y., and Handa, T. 1984, *Nature*, **310**, 568.
Sofue, Y., Inoue, M., Handa, T., Tsuboi, M., Hirabayashi, H., Morimoto, M., and Akabane, K. 1986, *Publ. Astron. Soc. Japan*, **38**, 475.
Sørenson, S.-A., Matsuda, T., and Fujimoto, M. 1976, *Astrophys. Space Sci.*, **43**, 491.
Tsuboi, M., Inoue, M., Handa, T., Tabara, H., and Kato, T. 1985, *Publ. Astron. Soc. Japan*, **37**, 359.
Tsuboi, M., Inoue, M., Handa, T., Tabara, H., Kato, T., Sofue, Y., and Kaifu, N. 1986, *Astron. J.*, **92**, 818.
Uchida, Y., and Shibata, K. 1985a, in *Unstable Current Systems and Plasma Instabilities in Astrophysics*, *IAU Symp. No. 107*, ed. M. R. Kundu and G. D. Holman (Reidel, Dordrecht), p. 287.
Uchida, Y., and Shibata, K. 1985b, in *The Origin of Non-radiative Heating/Momentum in Hot Stars*, ed. A. Underhill and A. G. Michalitsianos, NASA CP-2358 (NASA Scientific and Technical Information Branch, Washington, D.C.), p. 169.
Uchida, Y., and Shibata, K. 1985c, *Publ. Astron. Soc. Japan*, **37**, 515.
Uchida, Y., and Shibata, K. 1986, *Can. J. Phys.*, **64**, 507.
Uchida, Y., Shibata, K., and Sofue, Y. 1985, *Nature*, **317**, 699.
Yusef-Zadeh, F., Morris, M., and Chance, D. 1984, *Nature*, **310**, 557.
Yusef-Zadeh, F., Morris, M., Slee, O. B., and Nelson, G. J. 1986a, *Astrophys. J. Letters*, **300**, L47.
Yusef-Zadeh, F., Morris, M., Slee, O. B., and Nelson, G. J. 1986b, *Astrophys. J.*, **310**, 689.